NEOPLASIA
www.neoplasia.com

Volume 19 Number 11 November 2017 pp. 868–884 868

Directional Migration in Esophageal Squamous Cell Carcinoma (ESCC) is Epigenetically Regulated by SET Nuclear Oncogene, a Member of the Inhibitor of Histone Acetyltransferase Complex[1]

Xiang Yuan*,§,2, Xinshuai Wang*,§,2, Bianli Gu*, Yingjian Ma*, Yiwen Liu*, Man Sun*, Jinyu Kong*, Wei Sun*, Huizhi Wang‡, Fuyou Zhou† and Shegan Gao*,§

*Henan Key Laboratory of Cancer Epigenetics; Cancer Hospital, The First Affiliated Hospital, College of Clinical Medicine, Medical College of Henan University of Science and Technology, Luoyang, China, 471003; †Department of Thoracic Surgery, Anyang Tumor Hospital, Anyang, China, 455000; ‡Department of Oral Immunology and Infectious Diseases, University of Louisville School of Dentistry, Room 263D, 501 South Preston Street, Louisville, KY 40202, USA; §Department of Medical Oncology, Cancer Hospital, The First Affiliated Hospital, College of Clinical Medicine, Medical College of Henan University of Science and Technology, Luoyang, China, 471003

Abstract

Directional cell migration is of fundamental importance to a variety of biological events, including metastasis of malignant cells. Herein, we specifically investigated SET oncoprotein, a subunit of the recently identified inhibitor of acetyltransferases (INHAT) complex and identified its role in the establishment of front–rear cell polarity and directional migration in Esophageal Squamous Cell Carcinoma (ESCC). We further define the molecular circuits that govern these processes by showing that SET modulated DOCK7/RAC1 and cofilin signaling events. Moreover, a detailed analysis of the spatial distribution of RAC1 and cofilin allowed us to decipher the synergistical contributions of the two in coordinating the advancing dynamics by measuring architectures, polarities, and cytoskeletal organizations of the lamellipodia leading edges. In further investigations in vivo, we identified their unique role at multiple levels of the invasive cascade for SET cell and indicate the necessity for their functional balance to enable efficient invasion as well. Additionally, SET epigenetically repressed miR-30c expression by deacetylating histones H2B and H4 on its promoter, which was functionally important for the biological effects of SET in our cell-context. Finally, we corroborated our findings in vivo by evaluating the clinical relevance of SET signaling in the metastatic burden in mice and a large series of patients with ESCC at diagnosis, observing it's significance in predicting metastasis formation. Our findings uncovered a novel signaling network initiated by SET that epigenetically modulated ESCC properties and suggest that targeting the regulatory axis might be a promising strategy to inhibit migration and metastasis.

Neoplasia (2017) 19, 868–884

Abbreviations: ESCC, Esophageal squamous cell carcinoma; SET, SET nuclear oncogene; GEFs, Guanine nucleotide exchange factors; INHAT, Inhibitor of acetyltransferases; NAT, Natural antisense transcript

Address all correspondence to: Prof. Shegan Gao, Henan Key Laboratory of Cancer Epigenetics, Cancer Hospital, The First Affiliated Hospital, College of Clinical Medicine, Medical College of Henan University of Science and Technology, 24 Jinghua Road, Jianxi District, Luoyang, Henan, China 471003. or Fuyou Zhou, Department of Thoracic Surgery, Anyang Tumor Hospital, Anyang, China, 455000.
E-mail: gsgvicepresident@163.com

[1] This work was supported by grants from the National Natural Science Foundation of China (U1404817 for Xiang Yuan), Key project of science and Technology Department in Henan province (B20140763 for Xiang Yuan), Young academic leaders of Henan University of Science and Technology (for Xiang Yuan).

[2] *Xiang Y* and *Xinshuai W* as co-first authors.

Received 19 June 2017; Revised 4 August 2017; Accepted 4 August 2017

1476-5586
http://dx.doi.org/10.1016/j.neo.2017.08.003

Introduction

Directional cell migration is of fundamental importance to a variety of essential physiological processes as well as several disease processes including invasion of tumor cells into the surrounding stroma [1]. In an attempt to understand this complex process, migration has been viewed as a multiple-step cycle of morphological changes, which include acquisition of a highly polarized front-rear phenotype, coordination of membrane protrusion and retracting tail, reorientation of the Golgi, formation of stable focal adhesions and translocation of the cell body in the direction of the movement [2,3]. Furthermore, for productive, directional cell migration, the spatiotemporal integration of intracellular signaling components is of paramount importance. Among them, the plasma membrane receptors, adaptors, actin-severing proteins, small GTPases and their regulatory factor guanine nucleotide exchange factors (GEFs) have received a great deal of attentions [4,5].

Recently, experiments performed by Seo et al. [6] led to the discovery of a novel human cellular complex which inhibits the histone acetyltransferase (HAT) activity. This complex called INHAT (inhibitor of histone acetyltransferase), comprised of a group of acidic proteins that with novel "histone-masking" properties. Of considerable interest in this context, we specifically examined the role of the SET nuclear proto-oncogene (SET, also known as TAF-Iβ or I2PP2A), a defining member of the INHAT complex with diverse array of functions. However, in the nucleus, the best characterized functions is its core histone binding ability, and conceivably others by exhibiting histone chaperone activity, interacting with various factors such as DNA-binding proteins and negatively regulating of gene transcription [7]. Furthermore, SET oncoprotein, first identified as a translocation breakpoint-encoded protein in acute myeloid leukemia [8,9] is known to be over-expressed in several neoplasms. In this regard, recently, antagonism of SET using OP449 or FTY720, a specific, cell-penetrating peptide was reported to enhance the efficacy of tyrosine kinase inhibitors and overcomes drug resistance in malignancies [10].

To explore underlying mechanisms that mediate the effects of SET, we took a candidate gene approach and started by scrutinizing members of the DOCK180-related protein superfamily, of which a total of 11 mammalian members have been identified. This class of proteins emerged as a novel class of Rac/Cdc42 GTPase GEFs has been implicated in diverse cell type-specific processes, with some of its members (i.e., DOCK1 [11], DOCK3 [12], DOCK4 [13] and DOCK10 [14]) playing distinct roles in the migration and metastasis of diverse tumor types [15], including melanoma, breast cancer, head and neck squamous cell carcinoma, lung cancer and glioblastoma. Whether any of the DOCK proteins play a role in the migration or metastasis of ESCC has not been previously investigated. Owing to its actin-severing activity, cofilin, on the other hand, has emerged as one of the protein families playing an essential role in the dynamics of actin-based structures. And indeed, many literatures have implicated a crucial role for cofilin in establishing polarized cell morphology and chemotactic response which supports a central role for cofilin severing in defining the direction of stimulated cell motility [16,17].

Here we showed that, by coordinating the signaling events of DOCK7/RAC1 and cofilin, SET plays an essential role in the acquisition of a polarized phenotype and, accordingly, in directional cell migration. Moreover, SET epigenetically repressed miR-30c expression, which served as a direct regulator of the cross talk between DOCK7/RAC1 and cofilin. These novel findings demonstrate a novel role for SET oncoprotein in ESCC properties, and will have significant impact in understanding the epigenetic regulation of the INHAT class of protein in cancer cell biology.

Materials and Methods

Cell Culture and Cell Lines

The ESCC cells were grown in Dulbecco's modified Eagle's medium containing 10% fetal bovine serum (FBS), penicillin (100 U/ml), and streptomycin (100 mg/ml) (Sigma–Aldrich), at 37 C, in a humidified atmosphere containing 5% CO2.

Reagents and Antibodies

Rabbit anti-SET Antibody (A302-261A Bethyl Laboratories), Mouse anti–tubulin, Rabbit anti-FAK, Paxillin and Vinculin primary antibodies were used. Rabbit anti–phospho-Y397 FAK and mouse anti-paxillin phosphorylation were purchased from Abcam. TRITC-conjugated phalloidin, Anti-rabbit, anti-mouse, and anti-goat secondary antibodies conjugated with horseradish peroxidase (Invitrogen) were also used. FTY 720 was purchased from Tocris (6176).

SET Overexpression and Knockdown in ESCC Cell Line

The ESCC cells were transfected with SET DNA constructions using the PolyFect Reagent (Qiagen, Valencia, CA, USA), following the manufacturer's instructions. A SET human full-length cDNA clone (pCMV SPORT.6; NM_003011.3) was purchased from Invitrogen and transferred to a pcDNA3.1 vector (Invitrogen). SET knockdown in ESCC cell lines were transfected with double-stranded RNA oligonucleotides directed against SET (GS6418; Qiagen) or with a pool of four duplexes targeting SET (L-019586-00-0010, Dharmacon) using the HiPerFect transfection reagent (Qiagen), following the manufacturer's instructions. The siCONTROL AllStars siRNA Negative Control (Qiagen) was used as a negative siRNA control. Human DOCK7 and cofilin-specific shRNA and control pLKO.1 lentiviral vectors were purchased from GE Healthcare Dharmacon. Viral particles were prepared by transfecting HEK293T cells with psPAX2 packaging, pMD2.G envelope, and vectors using Lipofectamine 2000 transfection reagent (Life Technologies), as per the manufacturer's protocol. Virus-containing supernatant was collected and passed through 0.45-μm syringe filters before addition to target cells. Stably transfected cells were selected in 4 μg/ml puromycin.

Patients and Human Tissue

Two hundred patients with ESCC who underwent esophagectomy surgery from 2009 to 2014 at the First Affiliated Hospital of Henan University of Science and Technology and Anyang Tumor Hospital were investigated in this study. Adjacent tissue samples were obtained 3 cm distant to cancerous tissue. Thirty additional specimens were randomly selected during endoscopic examination from biopsy, and confirmed histologically as normal esophagus mucosa. Demographics (sex and age) and clinicopathologic features (differentiation status, lymphatic invasion, lymph node metastasis, TNM stage) were obtained from medical records. All of the surgical specimens were frozen immediately in liquid nitrogen and stored at −80 °C until use. Informed consent was obtained from all the patients. The study was approved by the Institutional Review Board of the University of Henan University of Science and Technology (HUST).

Quantification of Lamellipodia

Cells plated on coverslips were serum starved for 24 h and fixed with 4% formaldehyde in PBS, permeabilised with 0.1% Triton X-100 in PBS and incubated with Rhodamine-conjugated phalloidin (Molecular Probes) to stain F-actin. Nuclei were stained with DAPI. Images were acquired using a Zeiss Axiovert 200 M microscope. For

each experimental condition, images were taken in a random manner. Lamellipodia were traced using the ImageJ software. For each cell, the fraction of the cell perimeter that displays lamellipodia was calculated.

Cell Polarity and Migration Analysis

Transfected cells or RNAi treated cells were seeded on cover slips and cultured to confluency. Monolayers were scraped using a pipette tip and washed four times with pre-warmed medium. Transfected cells at the wound edge were identified by immunofluorescence imaging. Time-lapse live-cell images were captured every 1 min for 60 min for membrane dynamics analysis or every 10 min for 12 h for evaluation of cell migration. A set of cells was fixed and stained with rhodamine phalloidin for F-actin, anti-giantin for Golgi, and DAPI to visualize nuclei. Cells at the wound edge with Golgi polarized to the front-facing 120° sector were scored as positive for polarization.

Quantitative RT-PCR

RNA was isolated from the cells using the RNeasy kit (Qiagen) and from brain tissue (TRIzol) according to the manufacturer's instruction. 1 μg of DNase (Ambion)-treated RNA and oligo(dT) primers (Invitrogen) were denatured by incubating at 65 °C for 10 min. cDNA was synthesized using a reverse transcriptase (RT) kit according to the manufacturer's instructions (Roche). RT catalytic activity was inactivated by incubating the cDNA at 85 °C for 5 min. Real time PCR was performed using the SYBR Green quantitative PCR kit (Applied Biosystems).

Immunofluorescence Assay

Cells were fixed with absolute methanol at 20 C for 6 min, and blocked with 0.5% (v/v) Triton X-100 in phosphate-buffered saline (PBS) and 3% (w/v) bovine serum albumin (BSA). They were then incubated overnight with primary antibodies and washed three times with PBS. After incubation with an Alexa Fluor 546- and a FITC- or TRITC-conjugated secondary antibody for 1 h, the cells were stained with DAPI (Sigma–Aldrich) and visualized using a Zeiss Axiovert 40 CFL Microscope and Zeiss AxioVision 4.8.2 software.

Immunoblotting Assay

Protein concentration of the cellular extract was determined through the DC protein assay (Bio-Rad). Total proteins (30–50 mg) were resolved in SDS–PAGE and transferred to the PVDF membrane. The membrane was incubated overnight with primary antibodies, washed and incubated with secondary antibodies conjugated with horseradish peroxidase for 1 h. Bound antibodies were detected using an ECL Western blotting system (GE Health Care).

Histology and Immunohistochemistry

For immunohistochemistry analysis, tissue tumor microarray and paraffin sections were deparaffinized in xylene, rehydrated with ethanol gradient, treated using 10 mM sodium citrate buffer (pH 6) for antigen retrieval procedure according to standard method, blocked with 3% H2O2, permeabilized with immunohistochemistry (IHC) buffer (0.5% Triton X-100, 0.02% Tween-20/PBS), blocked with IHC buffer with 1% BSA and incubated with primary antibody overnight. (Primary antibodies are described in Antibodies for Western Blotting and Immunohistochemistry). Sections were washed three times with IHC buffer and incubated with biotinylated secondary antibody. Sections were washed three times with IHC buffer and incubated with streptavidin-HRP. Sections were washed three times with IHC buffer, one time with PBS, and the reaction was revealed using DAB peroxidase substrate kit (SK-4100, Vector Laboratories). Sections were counterstained with hematoxylin.

GTPase Activation Assay

Following treatment, cells were lysed on ice and active GTP-bound Rac1 was measured using the Active Rac1 Pull-Down and Detection Kit (Pierce-Thermo Fisher Scientific, Waltham, MA, USA) following the manufacturer's instructions.

Cytosol/Membrane Fractionation

Protein subcellular fractions were obtained using ProteoJET™ Cytoplasmic and Nuclear Protein Extraction Kit (Fermentas), according to the manufacturer's instructions. Samples were separated by SDS–PAGE and analyzed by immunoblotting. Membrane-to-cytoplasmic ratios of cofilin were assessed by densitometric analysis of immunoblots from the same exposure and normalized to control cells. For each protein, membrane and cytoplasmic lysates were run on the same gel.

Chromatin Immunoprecipitations (ChIP)

Briefly, 2×10^6 cells/10-cm dish were plated. 24 h after plating (or in the transfection experiments, 48 h post-transfection), cells were cross-linked in 1% formaldehyde for 10 min at room temperature with gentle shaking. The reaction was stopped by adding glycine to reach a 125 mM final concentration. Chromatin samples were precleared with 200 μl of a 50% slurry of Protein A-agarose/salmon sperm DNA (Upstate) for 1 h at 4 °C. The pre-cleared lysates were then divided into three aliquots and precipitated with the indicated antibodies (5 μg of Rabbit anti-SET Antibody (Bethyl), 5 μg of anti-acetyl-histones (Upstate), or with 5 μg of normal IgG (Santa Cruz) used as controls). Immune complexes were further incubated with Protein G-Sepharose beads (GE Healthcare) for 2 h at 4 °C. An aliquot of 40 μl of cell lysate was taken from diluted precleared samples prior to immunoprecipitations, and processed and treated as the immunoprecipitated sample. This served as the input control for the PCR component of the chromatin precipitations. 2 μl of immunoprecipitated DNA was used for real time PCR employing the SYBR Green quantitative PCR kit. For the analyses, we normalized the qPCR results first to GAPDH (an internal control gene) and then to input. For experiments with transfected cells, the data were presented as -fold enrichment of the PCR product in the cells transfected with siRNA targeting SET compared with cells treated with control siRNA.

Three-Dimensional Invasion Assay

The inverted collagen and fibronectin invasion assay was performed as described previously (Deakin and Turner, 2011). In brief, collagen I (PureCol; Advanced BioMatrix), mixed 5:1 with 10 × MEM, supplemented with 25 μg/ml fibronectin, was allowed to polymerize in 8-μm pore size transwell inserts (Corning) for 1 h at 37 °C in the absence of CO2. Cells were resuspended in serum-free medium and 10^5cells/ml and were seeded on the inverted transwell, on the filter surface. Cells were allowed to adhere for 1 h at 37 °C in the presence of CO2. Transwells were then placed in 1 ml serum-free medium, with the addition of 2 μM tubacin where stated. To establish a chemotactic gradient, medium supplemented with 10% fetal bovine serum and inhibitors where stated was placed in the upper chamber of the transwell. 3 d after seeding, cells were stained

with Calcein AM (Life Technologies) and visualized using a Zeiss Axiovert 200 M microscope (Zeiss) equipped with a × 2.5 objective. Images were acquired in 15-μm intervals up to 250 μm from the transwell surface as determined by phase-contrast imaging. Total cells in all images of the confocal series were quantified using ImageJ, and the relative percentage of cells invading ≥45 μm into the collagen and fibronectin plug was determined.

In Vivo Studies

All animal studies were performed in strict accordance with the recommendations in the guidelines for the Animal Care and Use Committee of The HUST. The protocol was approved by Science and Technology Commission of HUST Municipality. The rats were kept at 18 °C–26 °C on a 12 hours light and dark cycle with free access to water and standard rat chow. They were allowed to acclimatize for a minimum of 1 week. The environment was maintained at a relative humidity of 30%–70%. All surgery was performed under sodium pentobarbital anesthesia, and all efforts were made to minimize suffering. For the lung-seeding assays, clones injected into the tail veins of mice (1×10^6 total in 200 μl of PBS), Lungs were harvested 6 weeks post-injection, fixed in 4% paraformaldehyde/PBS, and the total number of metastatic lesions per animal lung was counted under a dissection microscope (Zeiss).

Microarray Analysis

Total RNA labeling and hybridization to Human Gene 1.0 ST Arrays (Affymetrix) were performed according to the Human Gene 1.0 ST Array kit protocol (Affymetrix). Genes that had a $\log_2$expression value of at least 4 under at least one of the treatment conditions were kept for downstream analyses. Differential expression estimation was based on a moderated *t* statistic (limma package) with subsequent calculation of the local false-discovery rate (lfdr) (locfdr package). Genes were classified as responders with an lfdr cutoff of 0.2. Gene Ontology (GO) and Kyoto Encyclopedia of Genes and Genomes (KEGG) pathway enrichment analyses were performed using a hypergeometric distribution test supplied by the GOstats package with a *P* value cutoff of 0.001.

Statistical Analysis

Values calculated from at least three independent experiments were compared by a Student's *t* test, and $P < .05$ was considered statistically significant. Error bars represent the standard error of the mean.

Results

A Novel Signaling Network Initiated by SET Oncoprotein Modulates the Mesenchymal Phenotype in Esophageal Squamous Cell Carcinoma

To select adequate cell lines for our experiments, we screened the expression levels of SET and manifestation of the phenotype in 12 Esophageal squamous cell carcinoma (ESCC) cell lines. It found that SET is widely expressed in a panel of conventional human ESCC cell lines, primarily in several cell lines with mesenchymal phenotype (Figure S1*A*).

Aiming to investigate the biological significance of SET to ESCC progression in vitro, we took advantage of cell lines expressed a negligible level of SET or endogenously expressed high levels of it, named EC-109/EC-1 (epithelial phenotype), and KYSE-150/KYSE-180 (mesenchymal phenotype), respectively, by stably expressed SET cDNA or transfected with two independent RNA interference constructs that depleted endogenous SET by at least 75% to mediate up (SET cells) or down-regulation of SET (Figure S1, *B* and *C*).

Subsequently, we compared the morphological phenotype of each cell lines by time-lapse microscopy. As shown in Figure 1*A*, EC-1 cell with ectopic SET expression transformed morphologically characterized by the extension of lamellipodia from a polarized elongated-shaped cell body than that of parental control (Figure 1*A*). Kyse-150 cells with SET down-regulation, however, exhibit aberrant cell architecture, thus, adopted a nonpolarized, rounded shape and were markedly inhibited in their ability to extend lamellipodia compared with the parental cells (Figure S1*D*). Similar results were obtained with SET-manipulated EC-109 and Kyse-180 cells versus their parental controls (Figure S1*D*), thus, ESCC cells prepared from these two strains (SET-knockdown Kyse-150 clones and ectopic expression of SET EC-1 clones) have been used throughout this study.

We conducted gene expression profiling using Affymetrix Human Gene arrays covering 28,869 genes in order to see whether the different EC-1 cell phenotypes resulting from ectopic expression of SET or control were reflected at the level of gene transcription. Overall, the analyses revealed modest changes in expression. Nevertheless, 211 genes displayed significantly decreased expression and 847 genes showed significantly increased expression after ectopic SET expression with the SET gene itself being one of the strongest responder (Figure 1*B*). Interestingly, a search for affected gene groups according to the classification of the KEGG pathways (Figure 1*C*) yielded the maps of focal adhesion, regulation of actin cytoskeleton and extracellular matrix (ECM)-receptor interaction. Furthermore, our data map to pathways in cancer. We also analyzed the list of SET-responding genes according to the GO classification (Figure 1*D*). In agreement with the KEGG analysis, genes involved in the "motility-dependent processes", "cellular microenvironment related genes" and "focal adhesion assembly" was enriched. In addition, overrepresentation of genes involved in "regulation of GTPase activity" and the "rearrangement of the actin cytoskeleton" were among the genes whose expression was increased as SET was ectopically expressed.

In view of the roles we had addressed for SET in mesenchymal cell properties, an enrichment of highly expressed genes function as the principal regulators of polarity and cytoskeletal rearrangements were of particular interests (Figure 1*B*), i.e., cofilin [16], one of the promising candidates owing to its ability to localize to sites of dynamic actin assembly and has known associations with cytoskeleton reorganization. On the other hand, we identified DOCK7 [18,19], a recently reported, but less well-known member of the DOCK180-related superfamily of GEFs, based on their evolutionarily conserved role in direct activation of the small GTPase RAC1, thus, assumed to exert its function during several fundamentally important motile processes. The differential expressed data were confirmed for a subset of genes, and DOCK7 and cofilin have been identified as robustly up-regulated genes in our signature both by real-time quantitative PCR (qPCR) and Western blot (Figure S2, *A* and *B*).

To elucidate the biological roles of DOCK7 and cofilin in our cell-context, we depleted the two proteins, either individually (knockdown cells) or in combination with each other, from SET cells by small interfering RNA (shRNA) (shDOCK7 and shcofilin) that we confirmed to be effective in reducing DOCK7 and cofilin protein levels (Figure S2*C*). We found that, inhibiting cofilin in SET cells abolished lamellipodia formation and cell elongation (Figure 1*E*). Similarly, cells in which DOCK7 is blocked, are unable to initiated an elongated

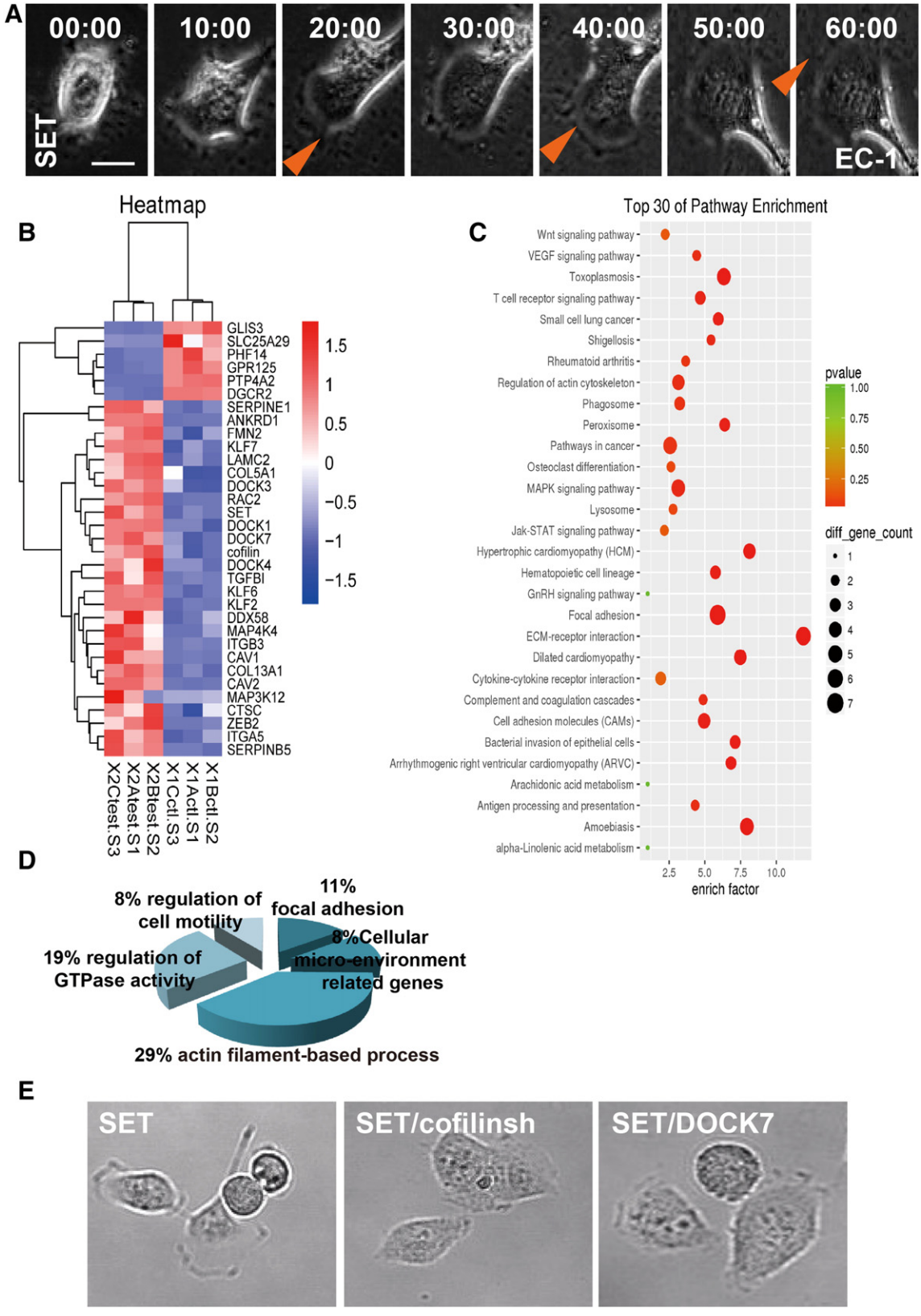

Figure 1. SET signaling network modulates the mesenchymal phenotype in ESCC. A. SET cells were plated sparsely and observed by time-lapse video microscopy. Intervals are indicated in hours above each column. Representative phase-contrast images showing lamellipodia morphology of migrating SET cell. Arrows mark the position of a protrusion from SET cell. B. Heat map illustrating the change in expression of up-regulated (red) and down-regulated (blue) genes belonging to the category "motility" according to GO after SET was ectopically expressed. C and D. Simplified KEGG and GO analysis of genes responding to SET over-expression. E. set cells or knockdown cells were plated sparsely onto dishes and observed for 48 hours by time-lapse video microscopy. Representative phase-contrast images showing morphology of migrating cells.

phenotype or extend a lamellipodium following SET up-regulation (Figure 1*E*).

In conclusion, we identify a SET-initiated signaling network involving DOCK7 and cofilin manipulation, which participates in ESCC cell elongation and lamellipodia formation.

SET Requires DOCK7 and Cofilin to Promote Front–Rear Polarization and Persistent Directional Migration in ESCC Cells

As a first approach, we analyze whole-cell motility from long time-lapse movies by tracking the movement of individual ectopic SET EC-1 cells (SET cells) or knockdown cells (SET/shDOCK7 and SET/shcofilin). SET cells displayed a highly elongated mesenchymal morphology and moved with a considerably higher Euclidean distance (Figure S3, *A* and *B*) and velocity (Figure S3*C*), typical of mesenchymal-mode movement. While inhibition of DOCK7 or cofilin alone or in combined in SET cells induced a dramatic cell morphological change from an elongated to a round phenotype with each cell populations exhibiting decreased mesenchymal motile plasticity (Figure S3, *A*–*C*).

To explore directional migration, we performed wound-healing assay and went on to analyze cell behaviors by tracking the movement of edge cells from different wounded monolayer. It observed that, SET monolayer had almost filled the wound space and the distance traveled was approximately 4 times more than that of controls at the same time interval (Figures 2*A* and S3D). Next, SET monolayer with DOCK7 and cofilin inhibition selectively was compromised in their ability to heal wound, with each cell population covered 45% and 30% of the denuded area, respectively. Interestingly, wound closure delay became significantly more evident in double knockdown monolayer, as only 20% of the wound area was covered (Figures 2*A* and S3D). This observation was confirmed by measuring the trajectory of each individual cell during a 12-h migration period by tracking its centroid from the time-lapse video. To clearly visualize the differences, cell movement paths were reproduced on composite panels (Figure 2*B*). Interestingly, we found that SET cells displayed much shorter net translocation (the shortest linear distance from the starting point to the end point of the time-lapse recording) than the control cells, which showed longer paths and migrated on a relatively straight line-track. While the expression of either DOCK7 or cofilin shRNA in SET-expressing edge cells resulted in behaviors whereby these cells migrated more randomly, with cells often changing directions as evidenced by wiggle line-tracks (Figure 2*B*). We then compare each healing pattern in greater quantitative detail. The degree of directional persistence as estimated by the index of the directionality of migration (i.e., the ratio of the net distance divided by the total distance traveled by the cell) significantly increased by the enforced expression of SET in EC-1 cells when compared with controls. Strikingly, however, the directionality was reduced upon the knockdown of DOCK7 or cofilin (Figure 2*C*). Moreover, SET cells had higher migratory velocity, which was again prevented when either DOCK7 or cofilin were inhibited (Figure 2*D*). Furthermore, by silencing both molecules, SET cells migrated with more significant deficiency in sustaining the directionality or velocity of the movement (Figure 2, *C* and *D*).

Persistent migration has been shown to require the establishment and coordination of active advancing dynamic, which is likely through the formation of a distinctly front-rear cell morphology as well as the repositioning of the condensed Golgi apparatus shortly before the commencement of advancement [5]. As an independent assessment of front–rear polarization, the axial ratio (length/width) of cells was calculated [20]. SET cells consistently had an elliptical factor of at least 1.5 (indicative of an elongated and polarized morphology), whereas knock down cells had a mean elliptical factor of 1 (Figure S3*E*), suggesting a loss of front–rear polarized morphology. To further define cell polarity, we assayed for Golgi apparatus polarization in cells migrating out of a wounded monolayer. Examination of the SET monolayer exhibited a typical fan-shaped broad lamellipodium facing into the wound and aligned Golgi projecting in the direction of migration. While SET cells with DOCK7 or cofilin blockade selectively or combined were impaired in the initiation or orientation of the dominant membrane extensions or cellular organelles toward the wound. Consequently, more than half of margin cells were not being correctly polarized, consistent with their decreased migratory parameters and the defect in wound closed-up (Figures 2*E* and S3*F*).

We further characterized the leading edge dynamics by measuring the percentage of cells that displayed fanning activity at 2-,4-, 6-, and 8-h time points and observed that, there was a steady increase in the percentage of fanning cells for SET cell layer, while the percentage in other layers remained low at each time interval: at the 2-h time point, 10% fanning SET cells was seen at edges, whereas at this time point, control wound edge had little fanning activity (2% fanning cells). At the 8-h time point, fanning SET cells reached 80%, while the percentage of fanning control cells remained low (20%). While treatment with DOCK7 or cofilin shRNA dramatically decreased the number of margin cells with fanning behavior, respectively at each time interval (Figure 2*F*). These results showed that the margin cells in SET layer responded to scratch-wounding faster and fanned earlier than in other monolayers.

Taken together, the ability to abrogate front–rear cell polarization formation, cellular organelles repositioning and fanning behavior in advancing cell edges by blocking DOCK7 and cofilin is consistent with the lack of directional persistence and the defect in wound closed-up in the movement of knockdown cells.

SET Regulates Localization and Activity of RAC1 and Cofilin

Impaired polarization and defects in the sustained directional migration pattern suggest alterations in the activity of the GTPases of the Rho family, as they are of the principal regulators of these processes [4]. Moreover, Docks are assumed to exert their function at the membrane via RAC1 activation [18]. Thus, the activity levels of RAC1 were measured through affinity precipitation assay with the isolated CRIB of Pak1, which specifically binds to activated GTP-bound RAC1. The assay revealed that the activity of RAC1 (activated GTP-bound RAC1) was strongly enhanced in presence of SET (Figure 3*A*). Treatment of kyse-150 cells with SET inhibitor, FTY720, on the other hand, led to a dramatic decrease of activated GTP-bound RAC1 time-dependently at least during the periods from 6 to 36 h (Figure 3, *B* and *C*). Of importance, the effect of SET depletion on RAC1 activities was also observed in other invasive ESCC cell lines, Kyse-180 (Figure S4, *A* and *B*), indicating that SET is involved in the activation of RAC1 in ESCC cell. In addition, we pursued whether DOCK7 as a potential RAC1 activator downstream SET in our system and found the increased activity of RAC1 seen upon SET up-regulation is eliminated under DOCK7-knockdown conditions (Figure 3*A*), establishing DOCK7 in the signaling pathway between SET and RAC1 activation.

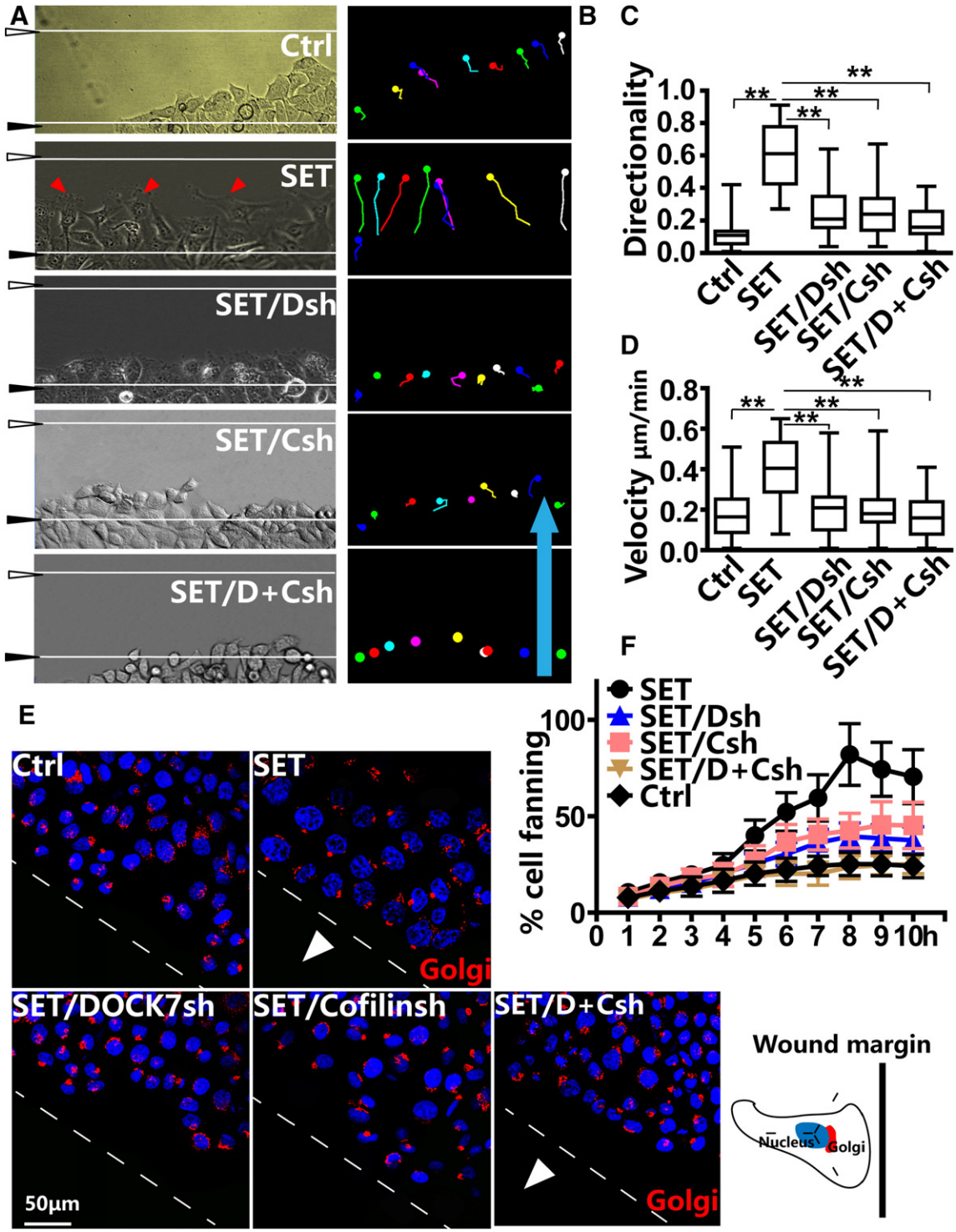

Figure 2. SET promotes front–rear polarization and migration directionality in a DOCK7 and cofilin-dependent manner. A. Confluent cells were scratched and recorded by time-lapse video microscopy. Representative images of cells at the wound edge were taken at 48 h after wounding. B-D. Quantification of migration after wound healing. Migration of individual cells at the wound edge was determined by centroid tracking. Representative tracks are shown. Cell migration velocity and directionality persistence were also calculated with Metamorph software. Migration data are shown as box plots. Error bars, SEM from three independent experiments. Statistical significance was determined by Student's t-test; (**) $P < .001$. E. Six hours after wounding, cells were fixed and stained with a Golgi marker (anti-Giantin, red) and nucleus (DAPI, blue). Percentage of cells exhibiting reoriented Golgi into the 120° sector facing the wound was quantified. F. Percentages of cells at the wound edge (n = 300) with fanning activity were scored at 2-, 4-, 6-, and 8-h time points. The proportions of leading-edge cells displaying lamellipodia were determined for three separate wound edges, 60 cells for each wound edge. For statistical results, Student's t test, $P < .05$.

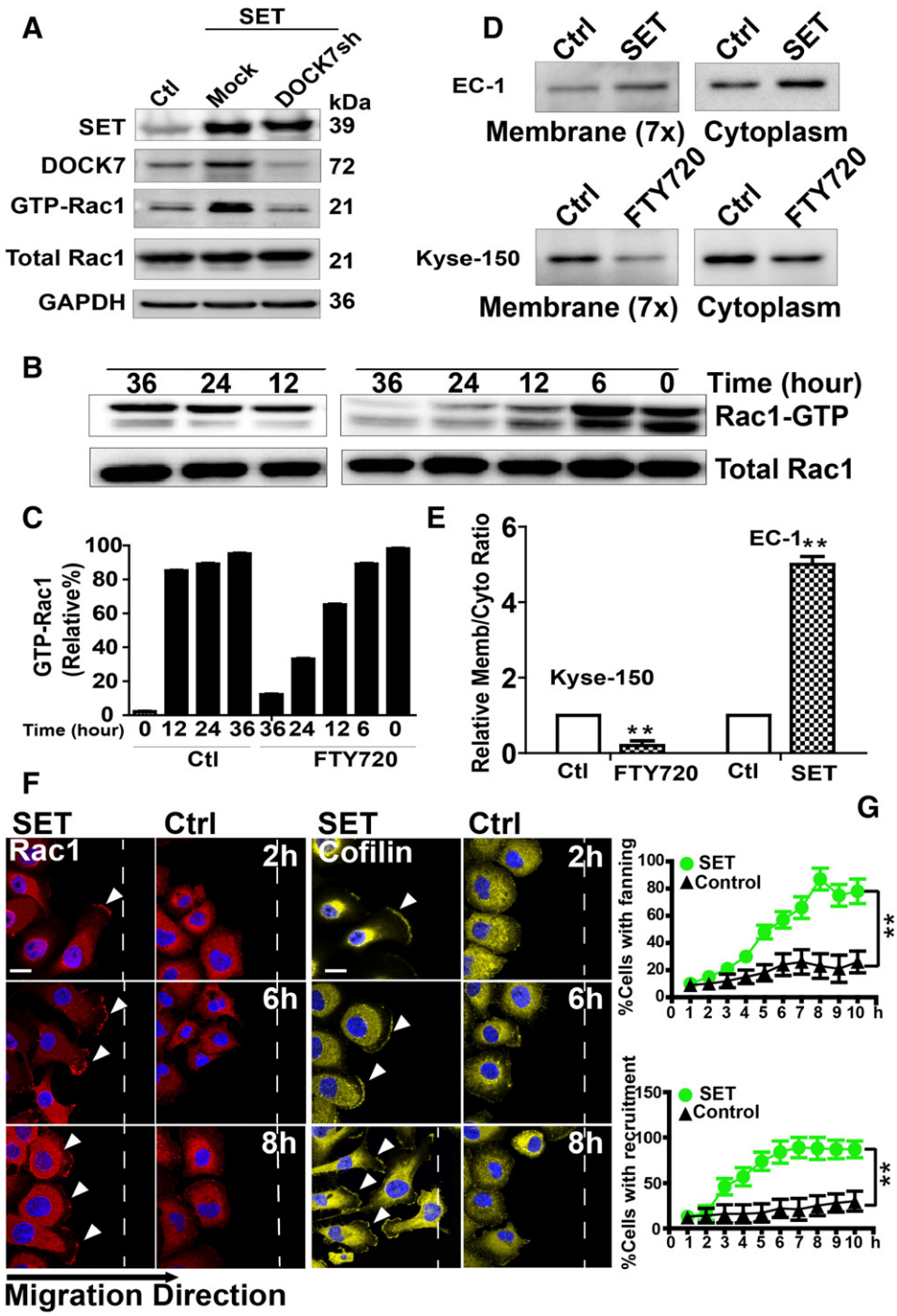

Figure 3. SET coordinates cell leading edge dynamics by controlling active RAC1 and cofilin levels. A. SET cells were transfected with mock or specific shRNA for DOCK7. At 48 h after transfection, cells were lysed and subjected to Western immunoblotting. Cell lysates were blotted for SET, DOCK7, and GTP/total RAC1. B. KYSE-150 cells left untreated or treated with 2 ng/mL FTY720 were collected at 0-36 h and processed for pull down assay. GTP-bound Rac1 was affinity precipitated with GST-CRIB, which specifically binds to GTP-bound Rac1, from cell lysates, and immunoblotted with an anti-Rac1 antibody. Total Rac1 level was comparable. C. Quantification of active Rac1 band intensity relative to total Rac1. Data represent mean ± SEM of three individual experiments. D and E. Membrane (concentrated seven-fold) and cytoplasmic fractions from SET EC-1 and FTY720 treated kyse-150 cells were immunoblotted for anti-cofilin antibody. Membrane-to-cytoplasmic (memb/cyto) ratios of cofilin was assessed (E) by densitometric analysis of immunoblots from the same exposure and normalized to control. For each protein, membrane and cytoplasmic lysates were run on the same gel. $^{**}P < .001$ by one-sample t test. F and G. Confluent cells were wounded, incubated for the indicated periods and subjected to immunostaining with anti-rac1, anti-cofilin antibody and DAPI (blue). Rac1 and cofilin were recruited to leading edges facing the wound in a time-dependent fashion. The results were from three independent experiments. Scale bar, 10 μm, (n > 100). The line chart (G) shows the percentage of cells with the puncta, and the percentages of cells (n = 300) that begin to fan and of those that have migrated into the scratch-wounds. Note that the percentage of cells with the presence of puncta closely correlated with the percentage of cells initiating fanning, in which the puncta were located along the leading edge of lamellipodia protrusions (F Arrowheads).

Because localization of Cofilin to the cell periphery is important for its activity [21], we postulated that SET might also affect cofilin membrane localization. To confirm this hypothesis, we performed cell fractionation experiments to isolate membrane and cytoplasmic fractions. We observed increased amounts of cofilin at the membrane in SET cells (Figure 3, *D* and *E*). Of interest, the cytoplasmic levels of Cofilin were also increased in SET cells, consisting with the observation that SET regulated the total protein levels of cofilin. On the basis of these results, we tested whether disrupting SET function would alter cofilin membrane localization by isolating membrane and cytoplasmic fractions from control and FTY720-treated kyse-150 cells. The results showed reduced cofilin at the plasma membrane in SET-inhibited cells compared with control kyse-150 cells (Figure 3, *D* and *E*).

We next localized RAC1 and cofilin by probing the two molecules in individual surrounding cells in scratched wound. There is extensive recruitment of RAC1 and cofilin along the margin in SET monolayer, where lamellipodia extension occurred and also toward the leading front of the cells migrating into the scratch site. While they were absent from the control monolayer, in which only diffuse cytoplasmic staining was observed (Figure 3*F*). We reasoned that, if SET affects the establishment of RAC1 and cofilin-dependent fanning phenotype as well as the formation of the RAC1 and cofilin-positive puncta at the leading edge, we would be able to establish a mechanistic relationship between fanning and puncta formation. To that end, we examined a large number of control and SET cells at wound edges at the 2-, 6- and 8-h time points after scratch-wounding. We observed that cells displayed the puncta were largely those that had just begun to fan and migrate into the scratch-wounds, which were frequently found among SET layers at the 2-h time points. Moreover, SET layers had considerable number of cells initiating fanning at the 6-h time point, and at this time interval a corresponding percentage of the cells are with the puncta. By the 8-h time point when the majority of the marginal cells in SET layer have formed broad lamellipodia and migrated into the scratch-wounds, the percentage of the cells with puncta had drastically increased. On the other hand, control edges at each time point showed little fanning activity and little evidence of puncta formation (Figures 3, *F–G* and S4*C*).

Our findings highlight that, the spatiotemporal regulation of RAC1 and cofilin activity at the leading edge may be the primary cellular event of SET cells that initiated advancing dynamics and determined migration.

DOCK7 or Cofilin Inhibition Results in Defects in Migration Machinery Components in SET Cells

In majority of mesenchymal-mode migration, the orchestration of the migration machinery components which are required for determining the migratory dynamics is achieved by reorganization of the actin and microtubule cytoskeleton as well as the turnover of cell–substrate adhesions [2]. Thus, we assess whether the alterations in leading edge dynamics observed when SET signaling was perturbed were reflected by changes in the cytoskeletal rearrangement.

Firstly, the leading edge of SET cells was well defined and contained a very dense population of actin bundles, spanning the length of the cell body and interacting with the cell cortex at the leading edge, a typical arrangement with highly dynamics for mesenchymal migration (Figure 4*A*). While the lack of interior actin stress fibers prevents cells from generating the traction forces needed for migration as in control (Figure 4*B*) and knock down cells (Figure 4*A*) which displayed pronounced rings of cortical actin structures. Second, the oriented microtubules aligned with the direction of migration as the lamellipodia became prominent in SET cells, however, tubules were poorly organized and less linear upon DOCK7 or cofilin inhibition or in control cells (Figure 4, *A* and *B*). Third, we assessed focal adhesions (FAs) formation by examining the FA-associated proteins Paxillin, Vinculin, and FA kinase (FAK). Focal complex-like structures were detected in the leading edge of SET migrating cells. Behind this region and under the cell body, we detected larger FAs of varying size that were often associated with actin stress fibers (Figure 4, *A* and *C–D*). In contrast, the general appearance of the FAs differed in the knockdown cells with decreased number and size of FAs was observed in the body (Figure 4, *A* and *C–D*). In addition, phosphorylation of FA complex is not only important for FA assembly but also for their turnover during cell migration. Western blot analysis revealed that there was a substantial increase in FAK Tyr397 and Paxillin phosphorylation in response to SET. However, depletion of DOCK7 or cofilin induced a substantial decrease in the phosphorylations (Figure 4*E*), typically indicated a change in the turnover and kinetics of adhesion assembly.

To determine whether the changes in cytoskeletal reorganization may, in part, account for the defects in migration, we analyzed the actin and focal adhesion structures in edge cells during the wound closure assay. Consistent with observations in sparsely plated cells, marginal cells in SET layers were asymmetric with a broad protrusive front containing large focal adhesions that capped a very dense population of actin bundles aligned in the direction of migration. While SET cells lacking RAC1 or cofilin do not protrude into the wound and displayed a nonuniform, diffuse focal adhesions staining, in which the actin-rich ruffles were neither densely packed, nor continuous, without a preferential orientation with respect to the leading edge (data not shown). We further went to assess whether these cytoskeletal alterations correlate with the distributions of active RAC1 and cofilin in fixed marginal cells. Obviously, the proper organized and well oriented actin bundles and FA structures was largely present in advancing cell edges that had proper peripheral recruitment of RAC1 and cofilin, thus, frequently present among the marginal cells of SET monolayer. Control marginal cells exhibited few actin- and FA-rich protrusions, intriguingly, in parallel with these, exhibited less obvious peripheral enrichment of RAC1 and cofilin (Figure S5, *A–C*).

DOCK7 and Cofilin Exert Differential Effects on Coordinating the Three-Dimensional (3D) Invasive Strategies as Well as Lung Seeding of SET Cell

Next, we went to determine the ability of SET cells to invade into a more in vivo relevant 3D microenvironmental setting, meanwhile questioning the potential roles that DOCK7 and cofilin played during the process.

Using collagen and fibronectin-rich plugs combined with time-lapse movies as an in vivo model, we found that, majority of SET cells invaded considerably further than the threshold distance of 45 μm into the 3D matrix three days post seeding. In fact, such cell type traveled almost throughout the entire height of the matrix with some cells invading up to 150 μm away from the expanding collective cell sheet (Figure 5*A*). In contrast, control cells appeared unable to invade efficiently, with only 10% of them detected above 45 μm, others failed to invade remained below the cutoff distance (Figure 5, *A* and $B_{a\text{-}b}$). While SET cell population was inhibited in their general invasion height when transfected with DOCK7sh, as the parental SET cell sheet invaded about 2.5 times deeper into the matrix than those with DOCK7 inhibition, although there was no obvious difference between the two cell populations in the proportion of the border cells traveling at the invasion front (Figures 5B_c

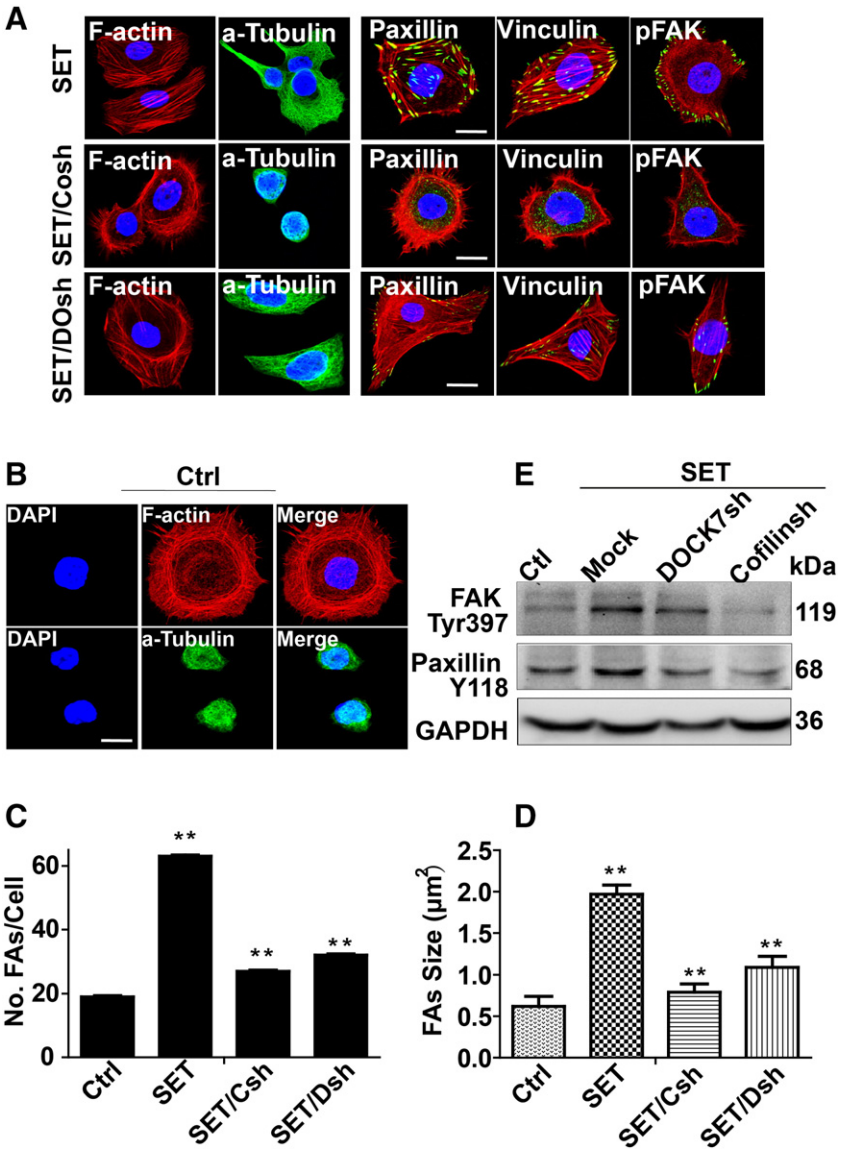

Figure 4. DOCK7 or cofilin inhibition results in defects in migration machinery components in SET cells. A and B. SET, control or knock down cells were plated onto glass coverslips and 48 h later were fixed and stained with for rhodamine-conjugated phalloidin and antibodies against microtubule, anti-paxillin, anti-vinculin, or anti-FAK. C and D. Quantification of the number and size of FAs. E. Tyrosine phosphorylation of focal adhesion components is altered in SET cells lacking DOCK7 or cofilin. Cell lysates of SET and knock down cells were collected and examined by immunoblot for pFAK (Y397) and paxillin (Y118). Results are from n = 3 independent experiments, means ± SD.

and S6 *A–B*). On the other hand, however, SET cell population with cofilin depletion seemed be decreased in both the degree of their invasion depth and the number of individual border cells (Figures 5B_d and S6 *A–B*). In addition, inhibition of both DOCK7 and cofilin expression reduced the SET cells' ability to exhibit invasive plasticity (Figures 5B_e and S6, *A–B*). Therefore, inhibition of either DOCK7 or cofilin expression both reduced the SET cells' ability to exhibit plasticity during 3D invasion in varying degrees, this effects were additive when both were targeted or inhibited simultaneously.

In the next set of experiments, we determined the metastatic potential of SET cells and assessed that, whether DOCK7 or cofilin could influence their ability to colonize the lung in vivo. To that end, we generated stable cell clones, including SET-expressing, controls, SET/DOCK7sh, and SET/Cofilinsh clones which were respectively injected into the tail vein of immunodeficient SCID mice for measurement of pulmonary colonization and verified six weeks post injection. Macroscopic analysis of the resected lungs revealed clear differences in the number of pulmonary colonization among the groups. Notably, SET clones-injected mice formed the most macroscopic pulmonary tumor nodules with 30-fold increases than mice injected with control clones. Moreover, nodules on the lung surface were significantly decreased in mice injected with SET/DOCK7sh, SET/cofilinsh or SET/FTY720 clones which bore 1.5-fold, 2-fold or 3-fold less nodules than in mice injected with parental SET clones, respectively (Figure 5, *C* and *E*). In addition, histological analysis of lung tissue by hematoxylin and eosin staining (H&E staining) confirmed the presence of metastases and revealed extensive infiltration of tumor cells throughout the lung tissue of mice that received an injection of SET cell clones, whereas the lungs isolated from mice that received SET/DOCK7sh, SET/cofilinsh or SET/FTY720 clones were significantly impaired in their ability to seed pulmonary metastases and exhibited much less evidence of

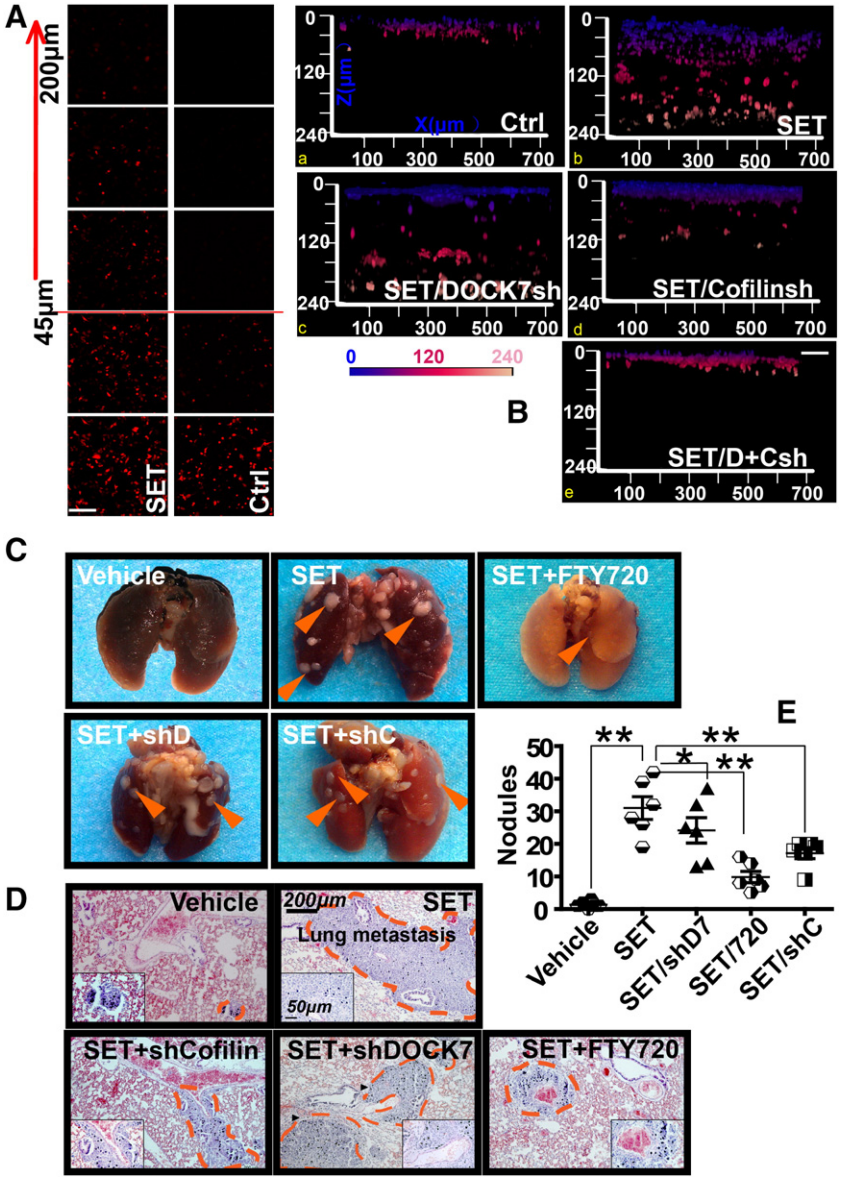

Figure 5. DOCK7 and cofilin exerts distinct effects on invasive properties of SET cells through 3D matrices. A and B. Serial optical sections were captured at 15-μm intervals and presented as a sequence in which the individual optical sections are placed alongside one another with increasing depth from lower to upper as indicated. Images at 0 μm indicate cells that came though the filter but did not enter the gel. Invasion capacity was expressed as a percentage of the total fluorescence intensity of all cells invading beyond 45 μm within the plug as shown in the bar graph. Confocal images taken at 15-μM intervals through the 3D matrix revealed significant increase in invasion for SET to control cells (A). Bar, 100 μm (average ± SEM, n = 3). X-Z stack view of SET cell invasion into 3D matrix revealed inhibition by cofilin or DOCK7 knockdown. Bar, 25 μm (B). At least three independent experiments were performed. C. Representative images of lungs harvested 6 weeks after tail vein injection of each cell clones (6 mice per group). The total number of lung colonies was quantified (E) using ImagePro Plus 6.0 software. D. Histological analyses of lung metastatic tumors by H&E staining. Circle indicates tumor sites. H&E staining showing that metastases in SET mice can be found residing inside blood vessels and invading the lung parenchyma. Enlargement of the circle regions in the top panels are shown in the bottom panels. Scale bars, 200 μm (middle) and 50 μm (bottom).

metastatic infiltrations (Figure 5*D*). We concluded that DOCK7 or cofilin inhibition hampered the potential ability of SET from forming pulmonary metastases in vivo.

Epigenetical Suppression of mir-30c Promoter was Functionally Important for the Biological Effects of SET in ESCC Cells

We next performed global miRNA profiling of SET cells. As shown, the dominant alteration after SET up-regulation was the down-regulation of a set of miRNAs (data not shown and Figure S7*A*). Especially, miR-30 family was of particular interests due to their well-known tumor-suppressing roles in various types of cancer, including ESCC. We further integrated the miRNA microarray results with several online computational algorithms (TargetScan, PicTar, and miRanda), and considered mir-30c as the candidate downstream SET due to its ability to target the 'seed' regions in the 3′UTR of DOCK7 and cofilin based on bioinformatic predictions (Figure 6*A*). Functional luciferase assays indicated that, the 3′ UTRs of DOCK7 and cofilin were repressed by miR-30c, but mutations of the predicted target sites completely abolished the repression, indicating that miR-30c directly targets DOCK7 and cofilin for suppression via their 3′ UTRs (Figure S7, *B* and *C*). Moreover,

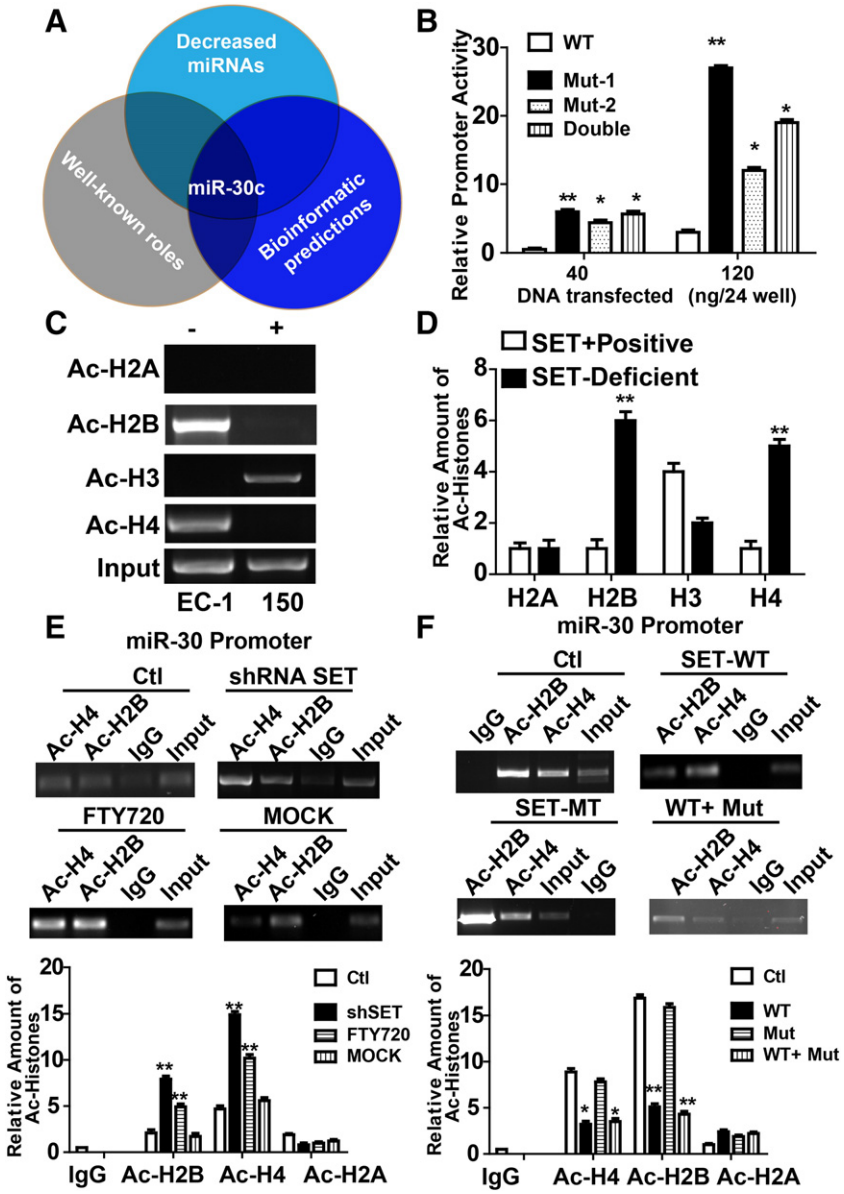

Figure 6. SET epigenetically controls the miR-30c promoter. A. Schema for identifying the motility-related targets of miR-30c. B. Effect of mutation of putative SET-binding sites (Mut1, Mut2 or double mutant) on miR-30c promoter activation measured by luciferase assay (*P < .05, **P < .001). C-D. ChIP analysis of SET-positive kyse-150 and SET-deficient EC-1 cells. Antibodies specific to acetylated histones H2A, H2B, H3 and H4 were used to test differential histone acetylation on the miR-30c promoter (C). qPCR analysis quantified the pulldown (D). E. Knockdown of SET results in hyperacetylation at the miR-30c promoter. Kyse-150 cells were transfected with shRNA targeting SET or control siRNA or treated with FTY720. Post-treatment, cells were processed for chromatin immunoprecipitation with anti-acetyl H2B, anti-H4 total antibody, or IgG (serving as a negative control). PCR was performed to amplify the promoter region of miR-30c and GAPDH (control). Pre-immunoprecipitated lysate served as input. qPCR analysis quantified the pulldown (lower panel). *P < .05, **P < .001. This figure is representative of three individually performed transfection experiments. F. Effect of wild-type and mutant SET on acetylation of histones H2B and H4 on miR-30c promoter in EC-1 cells measured by ChIP assay and qPCR.

the introduction of miR-30c mimic in ESCC cells inhibited the expression of DOCK7 and cofilin, whereas other miRNAs did not (data not shown). Furthermore, when SET was expressed in the ESCC cells, we found a significant reduction in miR-30c expression, and this result was coincident with greatly elevated levels of DOCK7 and cofilin as well as RAC1 activity, while the reconstitution of mir-30c in SET transfectant abrogated DOCK7 and cofilin expression and attenuated the increase in GTP-bound RAC1 (Figure S7, *A* and *D*). These results demonstrated that, miR-30c acts as an intermediate effector of SET, mediating its control activity on target levels.

Because SET is associated with the histone deacetylase complex [7], we examined the possibility that SET controls miR-30c epigenetically. We performed a Chromatin immunoprecipitation (ChIP) assay using two independently generated anti-SET antibodies. ChIP analysis showed that SET was bound to the miR-30c promoter (Figure S8, *A* and *B*). Furthermore, the inhibition of SET either by RNA interference or FTY720, a novel SET antagonist decreased the SET ChIP signal, indicating that the antibodies specifically recognized SET (Figure S8*C*). To further validate this interaction and examine its effect on miR-30c regulation, we carried out

mutation analysis. We identified two different clusters of putative SET-binding sites and mutated each of the binding clusters (Mut1 and Mut2) individually and also generated a double mutant. Each mutant led to miR-30 promoter activation, as measured by a luciferase assay with wild-type SET in Kyse-150 cells (Figure 6*B*), suggesting the importance of the binding sites for promoter repression. This is further supported by the observation that the double mutant did not show any additive effect (Figure 6*B*). Treatment with HDAC inhibitors (Apicidin, M344 and TSA) in Kyse-150 (SET^+) led to a 2- to 4-fold increase of miR-30 (Figure S8*D*). In contrast, in the SET-deficient cell lines, EC-1 (Figure S8*E*), miR-30 expression did not increase in response to the HDAC inhibitors, suggesting that the miR-30 promoter is controlled epigenetically and that the regulation is abrogated without SET. Indeed, luciferase reporter analysis in Kyse-150 cells showed a 7- to 10-fold increase in miR-30 promoter activation upon HDAC inhibitor treatment (Figure S8*F*). Moreover, the activation of promoters with mutated SET-binding sites decreased after HDAC inhibitor treatment (Figure S8*G*), suggesting that SET is involved in the epigenetic regulation.

On the basis of these results, we further tested whether SET affects the acetylation of one or more histones on the miR-30 promoter, which in turn could silence the gene. We carried out ChIP analysis using a series of antibodies recognizing acetylated histones and observed that H2B and H4 were more acetylated in SET-deficient EC-1 cells than in SET-positive Kyse-150 cells (Figure 6, *C* and *D*), indicating that SET is responsible for these acetylation changes. Subsequently, SET^+ Kyse-150 cells were challenged with shRNA directing against SET or the antagonist FTY720 and subjected to ChIP analysis. As indicated in Figure 6*E*. SET inhibition was found to cause substantial increases in the levels of H2B and H4 acetylation at the miR-30 promoter (Figure 6*E*). Moreover, the acetylation of H2B and H4 was lower when wild-type SET was expressed in EC-1 cells (Figure 6*F*). These data demonstrated that, SET negatively controls the miR-30c promoter by decreasing the acetylation of H2B and H4.

To explore the functional significance of mir-30c in the property of SET cells, we first studied the effects of its depletion using specific inhibitor and found that, silencing of mir-30c in EC-1 phenocopies the effect of SET on cell biological behaviors, including an increase in cellular protrusions, elongation, in vitro cell migration and in vivo 3D invasion were observed (Figure S9, *A*–*C*). On the other hand, concomitant DOCK7 and cofilin down-regulation impairs the phenotype established by mir-30 silencing (Figure S9, *A*–*C*). Subsequently, we asked whether mir-30c could override the oncogenic effects of SET in ESCC cells. For this purpose, mir-30c mimics were transiently transfected in SET-expressing ESCC cells. Remarkably, a decrease in cell mesenchymal phenotype and an impairment of in vitro cell migration and in vivo 3D ECM invasion were observed compared with parental SET cells (Figure S9, *D*–*F*). These experiments proved that mir-30c down-regulation is crucial and prerequisite for SET-mediated properties in ESCC cells, and apparently mediated these actions through targets mechanisms.

Evidence of the Existence of SET-Initiated Signaling Network in Human ESCCs

Considering the interconnections between SET and the modulated target signaling, we examined the clinical samples of ESCC for evidence of this signaling network. We measured their expressions by Q-PCR analysis in a panel of 200 pairs archival human esophageal samples, categorized as normal esophageal tissue (Normal), dysplastic, non-lymph node metastatic primary tumors (NESCC) or lymph node metastatic primary tumors (MESCC) and the paired lymph node. We observed that, compared with the paired healthy controls, SET expression levels were dramatically elevated in ESCC samples, especially in those with lymph node metastasis and the paired lymph node. Moreover, DOCK7 expression is up-regulated in ESCCs compared with healthy controls, and there appeared to be a progressive increase in DOCK7 expression levels from normal to metastatic samples. In addition, cofilin level is also significantly higher in lymph node metastases than in the localized ESCC and the normal tissues (Figure 7*A*), raising the possibility that the activation of SET-initiated signaling network associated with the progression to the metastatic phenotype. Whereas, clearly decreased level of mir-30c expression was observed in ESCCs relative to normal tissues, and the expression of mir-30c was also significantly different between cancerous tissues with lymph node metastasis and those without (Figure 7*A*). Afterward, Statistical analysis of Pearson's correlation in ESCCs indicated a strong negative correlation between the expression of mir-30c and SET-initiated signaling network (Figure 7*B*).

We further examined the expression of SET-initiated signaling network in tissue sections with IHC (Figure 7*C*). We found that the positive staining of SET was localized within the nucleus. In contrast, extensive cytoplasmic staining of DOCK7 and cofilin was observed in neoplastic samples (Figure 7*D*). A positive correlation between SET and DOCK7 and cofilin expression was also noted ($P < .05$, respectively). In addition, cells in the central tumor areas demonstrate moderate expression, whereas neoplastic cells at the tumor-host interface exhibited robust staining for the presence of SET and Cofilin in some cases suggesting that the SET pathway-positive cells might be mainly localized at the invading tumor front thus endowed with adverse pathologic phenotypes (Figure 7*D*). Consistent with our hypothesis, the activation of SET-initiated signaling network is correlated with an invasive and metastatic phenotype in human ESCCs (Figure 7*E*). Collectively, these data supported that, invasive ESCCs displayed evidence of the SET-initiated signaling network, reinforcing the role of this pathway as a potent driver of ESCC progression.

Discussion

Here, we provide evidence that the INHAT complex family subunit SET plays a critical role in coordinating front–rear polarity, Golgi reorientation and internal persistency of migration in ESCC cells (Figure 7*F*), whereas cells deficient in SET exhibit loss of polarity and display aberrant motility. That SET does so is an unanticipated function, for this INHAT family has been thought to be small size and lack of well-established signaling domains. Indeed, so far its only well-established role is implicated in chromatin-based pathways [22] including histone modification, mRNA stability, nucleosome assembly, and transcription. The etiopathological study provides an opportunity to uncover its other physiologically important functions. Using this rationale, our studied identify an entirely new and ubiquitous role for SET as a regulator of cell migration, thus adding a novel function to this list.

One of our main findings is that, alterations in the signaling of both DOCK7/RAC1 and cofilin are responsible for the aberrant phenotype of SET cells and both signaling always functioned synergistically and redundantly. First, DOCK7 shares functional

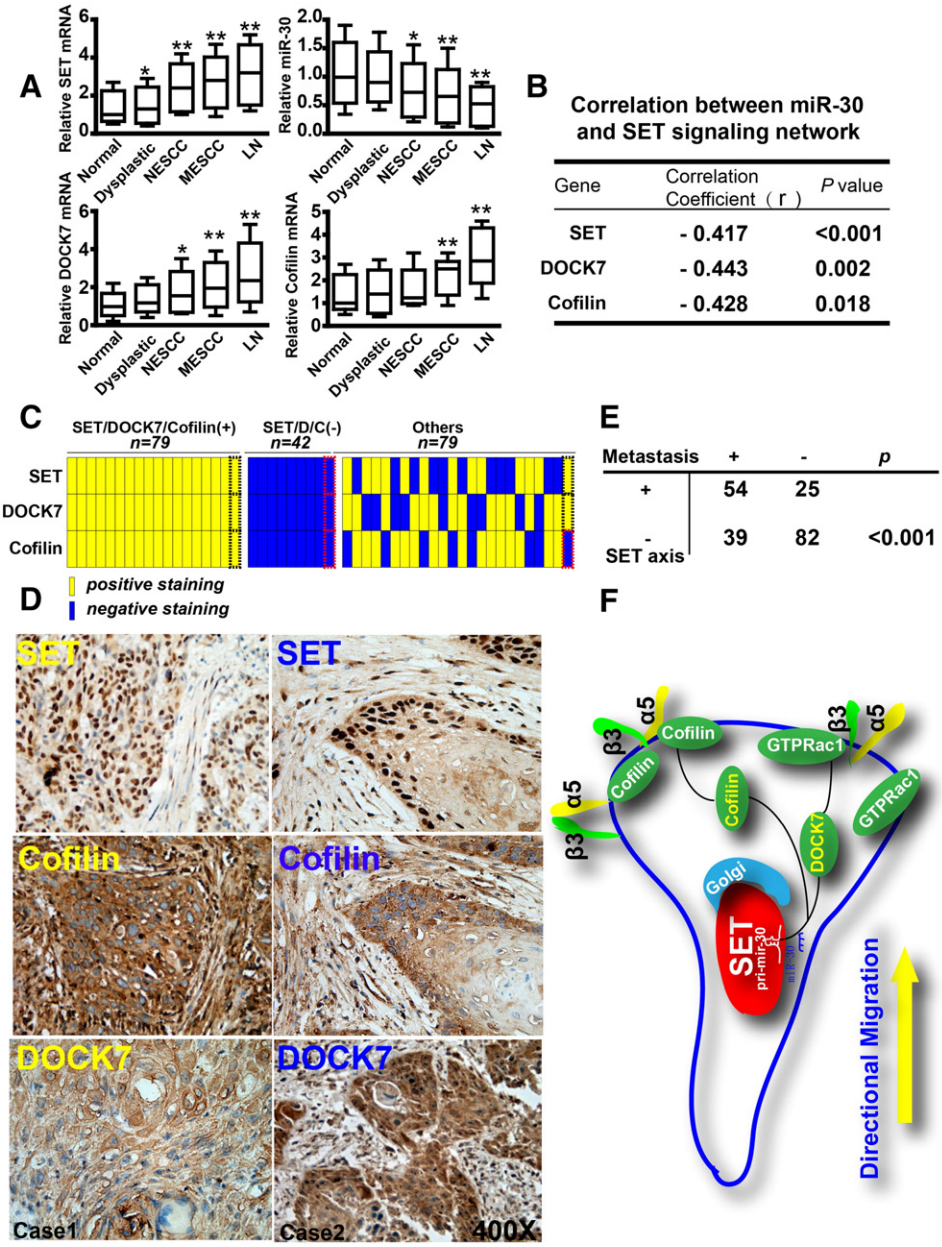

Figure 7. Evidence of the existence of SET signaling network in human ESCCs. A. Quantitative real-time PCR was performed to analyze mRNA levels of SET network (SET, DOCK7, cofilin, miR-30c) in a panel of 200 pairs archival human esophageal samples, categorized as normal esophageal tissue (Normal), dysplastic, non-lymph node metastatic primary tumors (NESCC) or lymph node metastatic primary tumors (MESCC) and the paired lymph node. *$P < .05$ **$P < .001$ by Student's t-test. B. Correlation between miR-30c and SET network relative expressions in a panel of ESCC samples, as quantified by qRT-PCR (Pearson's correlation, $P < .05$). C. A heatmap showing the result of IHC of SET, cofilin and DOCK7 in ESCC samples (n = 200). Yellow, positive staining; blue, negative staining in tumor tissue. D. Representative images of immunohistochemical staining of SET, cofilin and DOCK7 in two ESCC cases (Case 1 and case 2) indicate nuclear expression of SET, and cytoplasmic expression of cofilin and DOCK7. (400x) E. Correlations between the activation of SET signaling network and metastasis formation were analyzed in ESCCs by Chi-square test ($P < .001$). F. Scheme suggesting that SET promotes cell polarization and thus stimulates the directionality of cell movement by modulating DOCK7/RAC1 and cofilin signaling event. This presumably constrains spatial regulation of cofilin and rac1. Mir-30c facilitates a bridge between DOCK7 and cofilin. The fusiform cells represent cells moving in a mesenchymal mode.

properties of cofilin. In this regard, depletion of either DOCK7 or cofilin similarly led to a recovery of the morphological changes and persistent migration in 2D conditions. Moreover, in all cases a simultaneous depletion of both resulted in more pronounced phenotype than either one of the individual depletions. Furthermore, we provide the functional evidence for a synergistic interaction between them by showing that they two co-expressed in metastatic lesions of ESCCs. On the other hand, in reconstitution experiment, RAC1 is able to partially restore phenotypes in SET cells transfected with shRNAs targeting cofilin, suggesting that DOCK7 may be able to functionally compensate for loss of cofilin function in systems in which the two proteins are co-expressed.

The finding from our studies that SET promoted migration partially by activating the RAC1 pathway is somewhat surprising on a linear model of signaling where SET would be expected to be downstream of RAC1 and acted as a signaling amplifier for RAC1-mediated cell migration [23]. These seemingly contradictory observations may be explained if the relationship between SET and RAC1 is not considered as a simple linear pathway. Instead, the observations made here that SET depends on GEFs and leads to activation of the signaling complex provides a rationalization of why SET leads to increased activation of RAC1. In other cases, proteins such as SET and RAC1 may have more than one role in cells, because they have many potential binding partners and are likely to function as a part of large signaling complexes, thus, divergent results can be ascribed to tissue- or disease-specific context. Alternatively, provided the different migration approaches in both physiology and pathological conditions, therefore, contradictory results could be reconciled by a detailed analysis of random versus directional migration in multiple cell contexts.

The challenge will now be to decipher how cofilin and RAC1 activities are regulated coordinately in our system. It suggests that cofilin [24,25] and RAC1 [12] are regulated with high spatial and temporal precision and function in barbed end mobilization at the plasma membrane in a broad range of cell types. Consistently, in this study, both cofilin and RAC1 are recruited at the front edge of migrating SET cells. Why is that coordination of the activities of RAC1 and cofilin necessary? We postulate that, this pattern of surface dynamics might be related to the unique function of SET in promoting leading edge advancement. First, We scored edges for the percentage of cells with fanning activity and puncta formation (n = 300) at each time interval after scratch-wounding and found that the degree to which cells had initiated fanning at the SET wound edge correlated with the percentage of cells exhibiting RAC1 and cofilin puncta, suggesting a close correlation between the two events. Moreover, disruption of RAC1 and cofilin in SET cells impairs the ability of the two proteins to position themselves at the cell front, which is consistent with an appearance of lamellipodia extension delay there. The analysis of the ultrastructure of the actin and adhesion network at the leading edge where the function of the RAC1 and cofilin have been altered provides further information on how the two contribute toward maximizing cytoskeletal remodeling for protrusive force. The importance of the recruitments is further underscored by the observation that RAC1 and cofilin are transient recruited along the leading edge of small protrusions before they developed into broad lamellipodia. Thus, we reason that, whether these recruitments were the primary cellular event that initiates leading edge dynamics? It thus raised the possibility that: whether cells had earlier onset of recruitment also formed and protruded lamellipodia much earlier? Whether RAC1 and cofilin functioned in succession at different stages of lamellipodia formation in our cell-context? This is significant, as it has been shown that early cofilin-dependent barbed end transient is required for setting the direction of cell movement. Thus in this time-frame of fast kinetics, even a difference of seconds can be important. Thus, further work would be focused on the early phase of recruitments rates of these two proteins to the leading edge in presence of SET by transiently expressing fluorescent versions of full-length RAC1 and cofilin in these cells. In addition, for future studies it will be intriguing to visualize localized fluorescent edge intensity together with lamellipod dynamics to assess spatiotemporal correlation during cell migration.

It is widely established that, before to explore the 3D micro-environment, cells firstly have to degrade the matrices and generate a pore to finally undergo migration through it [26]. Our results reinforced the requirement of cofilin or DOCK7 in SET cells for their ability to function specifically for matrix remodeling or following locomotion, indicative of non-redundant cellular functions of the two in 3D filter assay. The most likely explanation of the discrepancies was that, different model environment are likely to give different environmental constraints, thus, yielded distinct physico-chemical requirements. i.e., in contrast to in vitro situation which mainly require migratory forces, under 3D conditions, tightly controlled polymerization of actin filaments to maintain actin flow are absolutely required for ECM degrading and deforming activities for path generation [27], which might be achieved by the activity of cofilin. There is substantial evidence showing that, this actin-severing protein increased the number of free barbed ends to initiate actin polymerization for actin-based protrusion in distinct subcellular compartments [21,28]. Such as invadopodium protrusion that is believed to be key process required for efficient invasion to occur. Although, it also suggested that cofilin is not necessary for invadopodium formation, but is required for maturation of fully functional invadopodia [29,30]. Which stages that cofilin principally functions in is out of the scope of this work, yet, the special dependence of 3D migration on actin remodeling combined with the reported importance of cofilin in the regulation of actin-based protrusion explained why 3D migration, in contrast to 2D, is more sensitively and specifically blocked by the inhibition of cofilin activity in our study. In addition, the fact that cofilin activity is less essential for SET cells to complete the following locomotion demonstrated that, cofilin primarily functions for specialized protrusive structures and not for broad protrusive activity involved in 3D cell invasion. Therefore, it is now clear that, regulatory cascade, such as cofilin, could exhibit different regulatory roles to the subtle variations and accomplish major changes in function that they required in responding to the physiological or other challenges. Upon reflection, this observation makes a great deal of sense. An interesting concept that has emerged from recent studies is that, when meeting an impasse, tumor cells will adopt a more exploratory migration phenotype to increase the likelihood of engaging blood or lymphatic vessels for intravasation [31,32]. The ability of cells to utilize different and favorable mode is postulated to due to the changes in the roles of the regulatory cascade or molecular repertoire, which gave advantages to tumor cells to adapt to different environmental constraints. Using this in vivo model system, we have identified unique roles for DOCK7 and cofilin at multiple levels of the invasive cascade for SET cell and indicate the necessity for the functional balance and extensive cross-talk between these closely related proteins might be required to fine-tune their optimal migration cellular functions.

In this work, we discovered a novel role of SET in regulating the expression of a tumor-suppressive miRNA, miR-30c, which has been extensively studied in the cancer biology. Our initial studies to understand how SET regulates miR-30c expression revealed that, class I and II HDAC inhibitors enhanced the expression of miR-30c in SET-positive cells. Therefore, reasoned that SET established the inactive state of the target genes by deacetylation of histones carried out by their associated HDACs. Subsequently, we carried out ChIP analysis and observed a specific association between HDAC2 and the miR-30c promoter in cells expressing SET. Moreover, we carried out co-IP analysis and observed the interaction between HDAC2 and

SET in ESCC cell. Further extensive experiments are obviously required to test whether the promoter recruit the SET-HDAC2 complex and led to reduced acetylation of core histones using promoter-specific primers. In this regard, the HDACs associated with SET may help deacetylate chromatin to establish the hypoacetylated state, which is subsequently occupied by SET.

In light of INHATs, by virtue of its ability to directly bind histone [33], however, it will be meaningful to examine whether SET was capable of directly repressing transcription. Our experiments revealed that chromatin targeting of SET repressed transcription in a dose-dependent manner. Of note, the proposed epigenetically regulatory role of SET in our study is consistent with the previous publications demonstrated that SET negatively regulates the transcription of array of targets, i.e. the specific neuronal differentiation markers [34], MAP1a and synapsin I; the estrogen receptor-regulated gene [33], EB1; the MYC target genes [35], Nucleolin, E2F2, and 5 s rRNA and the cellular detoxification enzymes [36], ALDH2 and GSTP1 via the histone acetylation inhibition of the gene promoters. The observation that another INHAT subunit LANP [37] directly influences the expression of the Nf-L chain gene by decreasing its promoter histone acetylation provide convincing evidence that INHATs influences the expression of genes by altering the histone acetylation status of the promoter region directly. Our work is to our knowledge the first example of INHATs shown to epigenetically regulate a miRNA implicated in cancer, providing new mechanistic insights. Moreover, since SET's association with leukemia [8] suggests a fundamental cellular function perhaps related to neoplasm. Our findings also imply that altered histone acetylation may serve as a plausible mechanism by which the oncogenic SET translocations contribute to neoplastic progression.

As with any seminal study, our work also raised several questions. It remains to be determined if SET's role was in a tissue- and cell-type-specific manner. Moreover, future studies investigating additional targets, as well as SET-interacting proteins, will enable us to more precisely define the cellular role of this protein in epigenetically transcriptional repression or the mechanisms involved. Furthermore, in light of the ability of the INHATs to associate with chromatin, one might expect that the activity of the INHAT complex and its targeting to chromatin must be tightly regulated, allowing the complex to perform its physiological functions while avoiding the serious consequences of over- or under-expression. Recent transcriptomics efforts have revealed that numerous protein-coding messenger RNAs have natural antisense transcript partners, most of which seem to be noncoding RNAs [38]. We have identified SET-AS, a natural antisense transcript, played a part in determining SET expression (unpublished data). SET-AS (RP11-545E17.3) was a putative novel transcript annotated by Havana. RP11-545E17.3 is a 544 bp RNA transcribed from the positive strand of chromosome 9, on the LOC100506100 locus (9q 34.11), 28 kb downstream of SET. We performed rapid amplification of cDNA ends (RACE) for directional sequencing of 5′ and 3′ ends and identified two splice variants for human SET-AS that overlap SET sense transcript. We found a poly-A tail and cap structure in the sequence, indicating that SET-AS is a fully processed transcript of RNA polymerase II. However, there is no apparent open reading frame. These data suggest that this previously unexamined noncoding RNA has a role in regulating SET and in driving ESCC's disease pathology.

Disclosure of Potential Conflicts of Interest

No potential conflicts of interest were disclosed.

Authors' Contributions

Conception and design: Xiang Yuan, Fuyou Zhou;

Development of methodology: Yiwen Liu, Jinyu Kong, Bianli Gu, Yingjian Ma, Xinshuai Wang, Man Sun;

Acquisition of data (acquired and managed patients, provided facilities, etc.): Fuyou Zhou, Wei Sun, Xinshuai Wang;

Analysis and interpretation of data (e.g., statistical analysis, biostatistics, computational analysis): Xiang Yuan, Jinyu Kong, Yiwen Liu, Bianli Gu;

Writing, review, and/or revision of the manuscript: Xiang Yuan;

Administrative, technical, or material support (i.e., reporting or organizing data, constructing databases): Xiang Yuan, Xinshuai Wang, Jinyu Kong, Yiwen Liu;

Study supervision: Shegan Gao, Huizhi Wang.

Acknowledgements

We wish to thank Zhengshan Chen in University of Pittsburgh and Qi Cao in University of California, Los Angeles for excellent technical help and for critical reading of an early version of the manuscript. We thank Dr. Shimada in Kyoto University for generously providing us with ESCC cell lines.

Appendix A. Supplementary Data

Supplementary data to this article can be found online at http://dx.doi.org/10.1016/j.neo.2017.08.003.

References

[1] Ridley AJ, Schwartz MA, Burridge K, Firtel RA, Ginsberg MH, Borisy G, Parsons JT, and Horwitz AR (2003). Cell migration: integrating signals from front to back. *Science* **302**, 1704–1709.

[2] Schwartz MA and Horwitz AR (2006). Integrating adhesion, protrusion, and contraction during cell migration. *Cell* **125**, 1223–1225.

[3] Chodniewicz D and Klemke RL (2004). Guiding cell migration through directed extension and stabilization of pseudopodia. *Exp Cell Res* **301**, 31–37.

[4] Settleman J (2001). Rac 'n Rho: the music that shapes a developing embryo. *Dev Cell* **1**, 321–331.

[5] Etienne-Manneville S (2008). Polarity proteins in migration and invasion. *Oncogene* **27**, 6970–6980.

[6] Seo SB, McNamara P, Heo S, Turner A, Lane WS, and Chakravarti D (2001). Regulation of histone acetylation and transcription by INHAT, a human cellular complex containing the set oncoprotein. *Cell* **104**, 119–130.

[7] Cervoni N, Detich N, Seo SB, Chakravarti D, and Szyf M (2002). The oncoprotein Set/TAF-1beta, an inhibitor of histone acetyltransferase, inhibits active demethylation of DNA, integrating DNA methylation and transcriptional silencing. *J Biol Chem* **277**, 25026–25031.

[8] Adachi Y, Pavlakis GN, and Copeland TD (1994). Identification and characterization of SET, a nuclear phosphoprotein encoded by the translocation break point in acute undifferentiated leukemia. *J Biol Chem* **269**, 2258–2262.

[9] von Lindern M, Breems D, van Baal S, Adriaansen H, and Grosveld G (1992). Characterization of the translocation breakpoint sequences of two DEK-CAN fusion genes present in t(6;9) acute myeloid leukemia and a SET-CAN fusion gene found in a case of acute undifferentiated leukemia. *Genes Chromosomes Cancer* **5**, 227–234.

[10] Neviani P, Harb JG, Oaks JJ, Santhanam R, Walker CJ, Ellis JJ, Ferenchak G, Dorrance AM, Paisie CA, and Eiring AM, et al (2013). PP2A-activating drugs selectively eradicate TKI-resistant chronic myeloid leukemic stem cells. *J Clin Invest* **123**, 4144–4157.

[11] Laurin M, Huber J, Pelletier A, Houalla T, Park M, Fukui Y, Haibe-Kains B, Muller WJ, and Cote JF (2013). Rac-specific guanine nucleotide exchange factor DOCK1 is a critical regulator of HER2-mediated breast cancer metastasis. *Proc Natl Acad Sci U S A* **110**, 7434–7439.

[12] Yang WH, Lan HY, Huang CH, Tai SK, Tzeng CH, Kao SY, Wu KJ, Hung MC, and Yang MH (2012). RAC1 activation mediates Twist1-induced cancer cell migration. *Nat Cell Biol* **14**, 366–374.

[13] Yu JR, Tai Y, Jin Y, Hammell MC, Wilkinson JE, Roe JS, Vakoc CR, and Van Aelst L (2015). TGF-beta/Smad signaling through DOCK4 facilitates lung adenocarcinoma metastasis. *Genes Dev* **29**, 250–261.

[14] Jaudon F, Raynaud F, Wehrle R, Bellanger JM, Doulazmi M, Vodjdani G, Gasman S, Fagni L, Dusart I, and Debant A, et al (2015). The RhoGEF DOCK10 is essential for dendritic spine morphogenesis. *Mol Biol Cell* **26**, 2112–2127.

[15] Gadea G and Blangy A (2014). Dock-family exchange factors in cell migration and disease. *Eur J Cell Biol* **93**, 466–477.

[16] Ghosh M, Song X, Mouneimne G, Sidani M, Lawrence DS, and Condeelis JS (2004). Cofilin promotes actin polymerization and defines the direction of cell motility. *Science* **304**, 743–746.

[17] DesMarais V, Ghosh M, Eddy R, and Condeelis J (2005). Cofilin takes the lead. *J Cell Sci* **118**, 19–26.

[18] Yamauchi J, Miyamoto Y, Chan JR, and Tanoue A (2008). ErbB2 directly activates the exchange factor Dock7 to promote Schwann cell migration. *J Cell Biol* **181**, 351–365.

[19] Murray DW, Didier S, Chan A, Paulino V, Van Aelst L, Ruggieri R, Tran NL, Byrne AT, and Symons M (2014). Guanine nucleotide exchange factor Dock7 mediates HGF-induced glioblastoma cell invasion via Rac activation. *Br J Cancer* **110**, 1307–1315.

[20] Grande-Garcia A, Echarri A, de Rooij J, Alderson NB, Waterman-Storer CM, Valdivielso JM, and del Pozo MA (2007). Caveolin-1 regulates cell polarization and directional migration through Src kinase and Rho GTPases. *J Cell Biol* **177**, 683–694.

[21] Mouneimne G, Soon L, DesMarais V, Sidani M, Song X, Yip SC, Ghosh M, Eddy R, Backer JM, and Condeelis J (2004). Phospholipase C and cofilin are required for carcinoma cell directionality in response to EGF stimulation. *J Cell Biol* **166**, 697–708.

[22] Fan Z, Beresford PJ, Oh DY, Zhang D, and Lieberman J (2003). Tumor suppressor NM23-H1 is a granzyme A-activated DNase during CTL-mediated apoptosis, and the nucleosome assembly protein SET is its inhibitor. *Cell* **112**, 659–672.

[23] ten Klooster JP, Leeuwen I, Scheres N, Anthony EC, and Hordijk PL (2007). Rac1-induced cell migration requires membrane recruitment of the nuclear oncogene SET. *EMBO J* **26**, 336–345.

[24] Dawe HR, Minamide LS, Bamburg JR, and Cramer LP (2003). ADF/cofilin controls cell polarity during fibroblast migration. *Curr Biol* **13**, 252–257.

[25] DesMarais V, Macaluso F, Condeelis J, and Bailly M (2004). Synergistic interaction between the Arp2/3 complex and cofilin drives stimulated lamellipod extension. *J Cell Sci* **117**, 3499–3510.

[26] Scott RW, Hooper S, Crighton D, Li A, Konig I, Munro J, Trivier E, Wickman G, Morin P, and Croft DR, et al (2010). LIM kinases are required for invasive path generation by tumor and tumor-associated stromal cells. *J Cell Biol* **191**, 169–185.

[27] Yu X, Zech T, McDonald L, Gonzalez EG, Li A, Macpherson I, Schwarz JP, Spence H, Futo K, and Timpson P, et al (2012). N-WASP coordinates the delivery and F-actin-mediated capture of MT1-MMP at invasive pseudopods. *J Cell Biol* **199**, 527–544.

[28] Sidani M, Wessels D, Mouneimne G, Ghosh M, Goswami S, Sarmiento C, Wang W, Kuhl S, El-Sibai M, and Backer JM, et al (2007). Cofilin determines the migration behavior and turning frequency of metastatic cancer cells. *J Cell Biol* **179**, 777–791.

[29] Oser M, Yamaguchi H, Mader CC, Bravo-Cordero JJ, Arias M, Chen X, Desmarais V, van Rheenen J, Koleske AJ, and Condeelis J (2009). Cortactin regulates cofilin and N-WASp activities to control the stages of invadopodium assembly and maturation. *J Cell Biol* **186**, 571–587.

[30] Yamaguchi H, Lorenz M, Kempiak S, Sarmiento C, Coniglio S, Symons M, Segall J, Eddy R, Miki H, and Takenawa T, et al (2005). Molecular mechanisms of invadopodium formation: the role of the N-WASP-Arp2/3 complex pathway and cofilin. *J Cell Biol* **168**, 441–452.

[31] Bear JE and Haugh JM (2014). Directed migration of mesenchymal cells: where signaling and the cytoskeleton meet. *Curr Opin Cell Biol* **30**, 74–82.

[32] Mladinich KM and Huttenlocher A (2013). WRAMPing up calcium in migrating cells by localized ER transport. *Dev Cell* **26**, 560–561.

[33] Kutney SN, Hong R, Macfarlan T, and Chakravarti D (2004). A signaling role of histone-binding proteins and INHAT subunits pp32 and Set/TAF-Ibeta in integrating chromatin hypoacetylation and transcriptional repression. *J Biol Chem* **279**, 30850–30855.

[34] Kim DW, Kim KB, Kim JY, Lee KS, and Seo SB (2010). Negative regulation of neuronal cell differentiation by INHAT subunit SET/TAF-Ibeta. *Biochem Biophys Res Commun* **400**, 419–425.

[35] Janghorban M, Farrell AS, Allen-Petersen BL, Pelz C, Daniel CJ, Oddo J, Langer EM, Christensen DJ, and Sears RC (2014). Targeting c-MYC by antagonizing PP2A inhibitors in breast cancer. *Proc Natl Acad Sci U S A* **111**, 9157–9162.

[36] Almeida LO, Goto RN, Pestana CR, Uyemura SA, Gutkind S, Curti C, and Leopoldino AM (2012). SET overexpression decreases cell detoxification efficiency: ALDH2 and GSTP1 are downregulated, DDR is impaired and DNA damage accumulates. *FEBS J* **279**, 4615–4628.

[37] Kular RK, Cvetanovic M, Siferd S, Kini AR, and Opal P (2009). Neuronal differentiation is regulated by leucine-rich acidic nuclear protein (LANP), a member of the inhibitor of histone acetyltransferase complex. *J Biol Chem* **284**, 7783–7792.

[38] Ponting CP, Oliver PL, and Reik W (2009). Evolution and functions of long noncoding RNAs. *Cell* **136**, 629–641.